∎ **Materials Chemistry** │*Very Important Paper*│

Di- and Tetracyano-Substituted Pyrene-Fused Pyrazaacenes: Aggregation in the Solid State

Lucas Ueberricke,[a] Ioana Ciubotaru,[a] Farhad Ghalami,[b] Felix Mildner,[a] Frank Rominger,[a] Marcus Elstner,[b] and Michael Mastalerz*[a]

Abstract: Five di- and tetracyano-substituted pyrene-fused pyrazaacenes were synthesized and studied as potential electron acceptors in the solid state. Single crystals of all compounds were grown and the crystal packing studied by DFT calculations (transfer integrals and reorganization energies) to get insight into possible use for semiconducting charge transport.

Introduction

Organic molecules with low lying LUMOs have many desirable properties, which make them an interesting class of materials for a wide range of applications, for example, as n-type semiconductors in organic field-effect transistors (OFETs),[1] as electron acceptors in solar cells or for organic light-emitting diodes.[1a,e,2] In the field of OFETs low LUMO levels favor electron injection and alignment with the work function of gold electrodes.[3] Low-lying LUMO levels further improve stability by reducing the decomposition of negatively charged species on exposure to oxygen or water and are therefore valuable for operating organic electronic devices under ambient conditions.[1a,4] However, only a few n-type semiconductors with high electron mobility have been reported so far [e.g., aromatic diimides ($\mu_e = 1.30$–8.60 cm^{2}V^{-1}s^{-1}),[5] tetraazapentacenes ($\mu_e = 11.0$–13.3 cm^{2}V^{-1}s^{-1}),[6] cyano-terminated quinoidal terthiophenes ($\mu_e = 3.00$ cm^{2}V^{-1}s^{-1}),[7] and B-N-fused dibenzoazaacene ($\mu_e = 1.60$ cm^{2}V^{-1}s^{-1}).[3a] The design and synthesis of new electron-transport materials therefore remains an attractive goal. The general strategy is to attach or include electron-withdrawing groups or atoms (e.g., halogens, boron, cyano or acyl groups) to or in an aromatic backbone.[1a,7–8] In this context, pyrene-fused pyrazaacenes (PPAs) are especially promising due

to their high stability and their already considerably low LUMO energies.[3b,9] By attaching cyano groups to PPAs, electron acceptors that fulfill certain criteria to be attractive for organic electronics should be readily available by condensation reactions. Surprisingly, to date only a few cyano-substituted PPAs have been reported. To the best of our knowledge, the first such derivatives were mentioned in 1975 by Wöhrle et al.[10] The synthesis as well as IR spectra and UV/Vis spectroscopic analysis of **PQDC** and **H-PPQTC** were described. These compounds were studied for the formation of amino-iminopyrazines as valuable precursors for phthalocyanines, which was realized by Nardi et al. for **H-PPQTC** in 2014 on Cu surfaces.[11] A *tert*-butyl-substituted derivative of **PPQTC** was synthesized by Liu and co-workers in 2011.[12] **tBu-PPQTC** and **H-PPQTC** were thoroughly investigated by UV/Vis, photoluminescence, and cyclovoltammetry, which clearly identifies these compounds with LUMOs comparable to that of PCBM$_{61}$ as potential electron acceptors for applications in organic electronics. In the same year Abdel-Razik described the synthesis of the larger congener **tBu-QPPTC** as precursor for polymer networks based on phthalocyanine formation.[13] Mateo-Alonso obtained soluble derivatives of both core structures by attachment of triisopropylsilylethynyl substituents to the 2,7-positions of the pyrene core.[3b]

Besides the molecular electronic structure, intermolecular orbital overlap plays a crucial role for charge transfer. Therefore, knowledge of the molecular arrangement of fused aromatic molecules in the solid state is of utmost importance to calculate transfer integrals for charge transfer to evaluate the potential of these structures for electronic applications in more detail.[14]
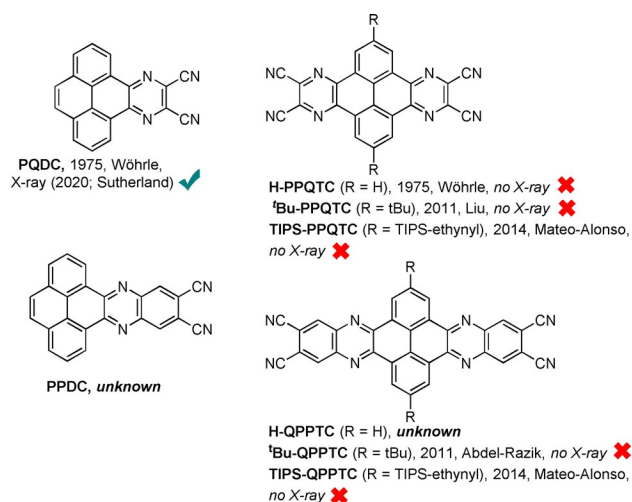
Despite the attractive low-lying LUMOs of the few literature-known cyano PPAs of Scheme 1, no X-ray structures giving more detailed information about the above-mentioned possible arrangement were described to date. The only exception is **PQDC**, for which a solid-state structure was described recently.[15] This contribution had a different focus, and therefore no discussion of transfer integrals was done. Because of the high

[a] L. Ueberricke, I. Ciubotaru, F. Mildner, Dr. F. Rominger, Prof. Dr. M. Mastalerz
Organisch-Chemisches Institut, Ruprecht-Karls-Universität Heidelberg
Im Neuenheimer Feld 270, 69120 Heidelberg (Germany)
E-mail: Michael.mastalerz@oci.uni-heidelberg.de

[b] F. Ghalami, Prof. Dr. M. Elstner
Institut für Physikalische Chemie, Karlsruher Institute of Technology (KIT)
Kaiserstrasse 12, 76131 Karlsruhe (Germany)

Supporting information and the ORCID identification number(s) for the author(s) of this article can be found under:
https://doi.org/10.1002/chem.202002382.

Chemistry–A European Journal

Full Paper
doi.org/10.1002/chem.202002382

Chemistry Europe
European Chemical
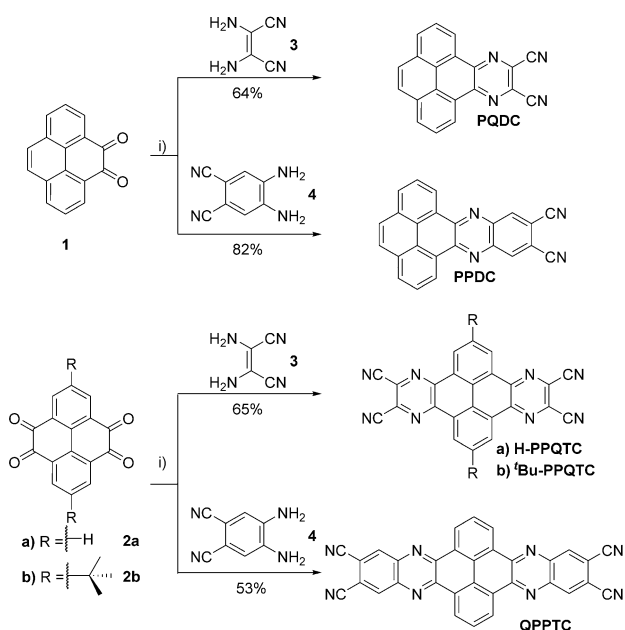Societies Publishing

Scheme 1. Overview of literature-known cyano-substituted PPAs.

potential of such cyano PPAs and the lack of detailed structural information in the solid state, we revisited this class of compounds to grow single crystals, study packing, and calculate transfer integrals.

Results and Discussion

Synthesis and characterization

Phenanthroquinoxalino dicarbonitrile (**PQDC**) and phenanthro-phenazine dicarbonitrile (**PPDC**) was synthesized by acid-catalyzed condensation of pyrenedione **1**[16] with 2,3-diaminomalo-nitrile **3** and 4,5-diaminophthalonitrile **4**, respectively (Scheme 2).[3b] Pyrazinophenanthroquinoxaline tetracarbonitrile derivatives **H-PPQTC** and **tBu-PPQTC**, as well as quinoxalino-

phenanthrophenazine-tetracarbonitrile derivative **QPPTC** were synthesized accordingly from pyrenetetraone **2 a**.[16–17] After the reaction the crude products were isolated by filtration and washed with methanol. Subsequently, **PQDC**, **H-PPQTC**, and **tBu-PPQTC** were heated to reflux in 30% nitric acid and filtered while still hot.[11]

During this step a color change from dark brown to beige was observed. After filtration and washing with water and methanol the solids were extracted in a Soxhlet apparatus to obtain **PQDC** as a metallic golden powder and the two **PPQTC** derivatives as light-yellow solids. The yields of the three compounds were 64–65%. **PPDC** was purified by washing with THF and methanol and isolated as an orange powder in 82% yield. Soxhlet extraction with THF gave **QPPTC** as yellow powder in 53% yield. **PPDC** could be further purified by sublimation in a kugelrohrofen at 300 °C and (5–8)×10⁻³ mbar. **PQDC** and the two **PPQTC** derivatives could be sublimed under similar conditions, but showed additional signals in the ¹H NMR spectra indicating decomposition (see Supporting Information).

All compounds were fully characterized by ¹H and ¹³C NMR spectroscopy, IR spectroscopy, HRMS, and elemental analysis (for details, see Supporting Information).

Optoelectronic properties

All compounds were studied by UV/Vis and fluorescence spectroscopy in dichloromethane or *ortho*-dichlorobenzene (*o*DCB) in the case of **H-PPQTC** for solubility reasons (Figure 1). Absorption spectra of **PQDC** and **H-PPQTC** have already been reported,[10] but are included in the discussion as well. Pronounced differences for di- and tetrasubstituted compounds were observed, whereas similar spectra for di- and tetracyano compounds were obtained. **PQDC** shows absorption peaks at 447, 354, 313, 284, and 258 nm corresponding to n–π* and π–π* transitions.[10,18] Due to the elongation of the aromatic core, a bathochromic shift of the longest-wavelength absorption peaks towards $\lambda_{abs} = 485$ nm is observed. Two peaks at 348 and 333 nm are much better resolved compared with **PQDC**. Both compounds have very similar emission spectra with a

Scheme 2. Synthesis of di- and tetracyanopyrazines **PQDC**, **PPDC**, **H-PPQTC**, **tBu-PPQTC**, and **QPPTC**. Conditions: i) EtOH/AcOH (1:1), Ar, 80 °C, 11–16 h.
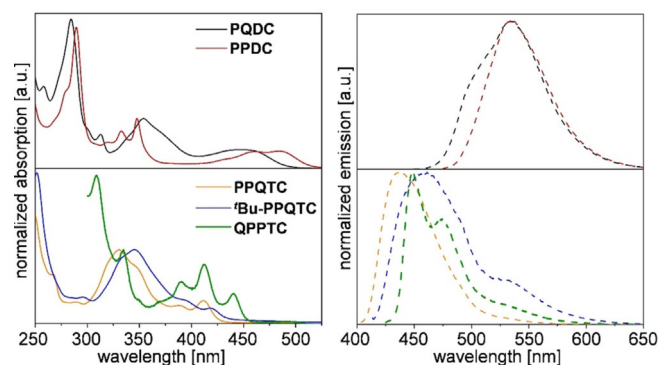

Figure 1. Absorption and emission spectra of **PQDC**, **PPDC**, **H-PPQTC**, and **tBu-PPQTC**, measured in CH₂Cl₂ (1×10⁻⁶ mol L⁻¹) at RT and of **QPPTC** measured in *o*DCB (1×10⁻⁶ mol L⁻¹) at RT.

Chemistry–A European Journal

Full Paper
doi.org/10.1002/chem.202002382

Chemistry Europe
European Chemical
Societies Publishing

maximum at $\lambda_{ex} = 533–534$ nm and a blueshifted shoulder at 510 nm for **PQDC**, resulting in Stokes shifts of $E_{Stokes} = 3609$ cm^{-1} for **PQDC** and $E_{Stokes} = 1891$ cm^{-1} for **PPDC**, indicating a decrease of reorganization energy from the transition of the ground state to the first excited state.[19] This might be explained by the larger aromatic system of **PPDC**, which is less influenced by structural change when excited. Photoluminescence quantum yields (PLQY) were 31% for **PQDC** and 22% for **PPDC**. Both **H-PPQTC** and **tBu-PPQTC** have a weak absorption maximum at $\lambda_{abs} = 426$ nm and $\lambda_{abs} = 437$ nm and a broad absorption band at $\lambda_{abs} = 330$ nm and $\lambda_{abs} = 345$ nm, respectively. The π–π* transition bands (≈ 215 nm) are significantly reduced compared to those of the dicyano compounds **PQDC** and **PPDC**. **H-PPQTC** emits at $\lambda_{em} = 437$ nm (PLQY of 37%), resulting in a Stokes shift of $E_{Stokes} = 1448$ cm^{-1}. For **tBu-PPQTC** the emission maximum is redshifted compared to **H-PPQTC** by 24 nm to $\lambda_{em} = 461$ nm and shows an additional peak at 529 nm, which might be due to excimer formation. The corresponding Stokes shift ($E_{Stokes} = 2231$ cm^{-1}) is larger than that of **H-PPQTC** (1448 cm^{-1}), and the PLQY (15%) was lower than that of **H-PPQTC** (37%). Both values are in agreement with data reported in the literature.[12] **QPPTC** shows distinct absorption maxima at $\lambda_{abs} = 440, 412, 390, 335,$ and 309 nm. The emission maximum at $\lambda_{em} = 449$ nm with a small Stokes shift of $E_{Stokes} = 455$ cm^{-1} is indicative of the formation of a J-aggregate.[20] A second emission maximum is found at $\lambda_{em} = 475$ nm with a shoulder at approximately 526 nm. The PLQY was 8%. The optical bandgaps estimated from the onset wavelength lie between 2.4 eV (**PPDC**) and 2.9 eV (**H-PPQTC**).

All compounds were studied by cyclovoltammetry in dichloromethane, except **QPPTC**, which was studied in oDCB (Figure 2). For **PQDC** only one quasireversible reduction potential at $E^{red} = -1.42$ V was observed, whereas for the other three compounds two potentials were detected.

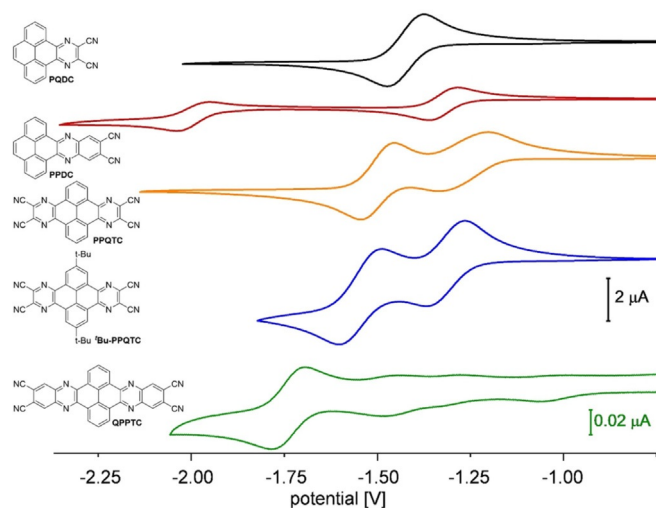For **PPDC**, the first reduction potential was found at $E^{red,1} = -1.32$ V and the second at $E^{red,2} = -1.99$ V. Both **H-PPQTC** ($E^{red,1} = -1.26$ V; $E^{red,2} = -1.49$ V) and **tBu-PPQTC** ($E^{red,1} = -1.31$ V and $E^{red,2} = -1.54$ V) showed similar reduction potentials, which is in agreement with prior reported values in the literature.[12] For **QPPTC** the solubility is very low, even in oDCB, and therefore only a signal of low intensity could be found. **QPPTC** has one quasireversible reduction potential at $E^{red} = -1.74$ V. From the first reduction potentials the electron affinities were estimated by the commonly used expression $EA = -(E^{red,1} + 4.8)$ eV. They are 3.1 eV for **QPPTC** and 3.4–3.5 eV for the other four compounds.

DFT calculations (B3LYP/6-311 + +G**) for all compounds were done to compare frontier molecular orbitals of these electron-acceptor compounds (Figure 3). The HOMO of **PQDC** is found at $E_{HOMO} = -6.6$ eV with orbital coefficients that are larger on the pyrene core than on the pyrazine units and the cyano substituents. This is similar for the HOMOs of all other compounds. The LUMO energy is calculated to be $E_{LUMO} = -3.3$ eV, and here the orbital coefficients are mainly located at the pyrazine unit and the substituents. Again, this is similar for all other compounds of this series. **PPDC** has one more fused ring between the pyrene core and the pyrazine unit, and thus the gap between HOMO and LUMO is smaller with a slightly stabilized LUMO at $E_{LUMO} = -3.5$ eV and a destabilized HOMO at $E_{HOMO} = -6.5$ eV. In comparison with **PQDC**, for **H-PPQTC** with two pyrazine units and four cyano substituents, both LUMO and HOMO are significantly stabilized ($E_{LUMO} = -3.9$ eV and $E_{HOMO} = -7.4$ eV). The frontier molecular orbital energies between **PPDC** and the larger **QPPTC** are comparable, with $E_{LUMO} = -3.9$ eV and $E_{HOMO} = -7.3$ eV. The energy levels of the two larger compounds **H-PPQTC** and **QPPTC** are quite comparable. The introduction of two tert-butyl groups at the pyrene 2,7-positions (**tBu-PPQTC**) destabilizes the LUMO by about $+0.2$ eV to $E_{LUMO} = -3.7$ eV. This is slightly lower than that of the corresponding triisopropylethynyl-substituted tetracyano derivatives ($E_{LUMO} = -3.4$ to -3.5 eV).[3b] The optoelectronic properties are summarized in Table 1.

Figure 2. Cyclic voltammograms of **PQDC**, **PPDC**, **H-PPQTC**, **tBu-PPQTC** (CH$_2$Cl$_2$, nBu$_4$NPF$_6$ (0.1 M)), and **QPPTC** (oDCB, nBu$_4$NPF$_6$ (0.1 M)), measured at room temperature with a Pt electrode, an Ag/Ag$^+$ pseudo-reference electrode, and Fc/Fc$^+$ as internal reference (scanning speed: 50 mV s^{-1}). Note, that the scale of the y axis of **QPPTC** is different from that of the other compounds because of the much lower signal intensity.
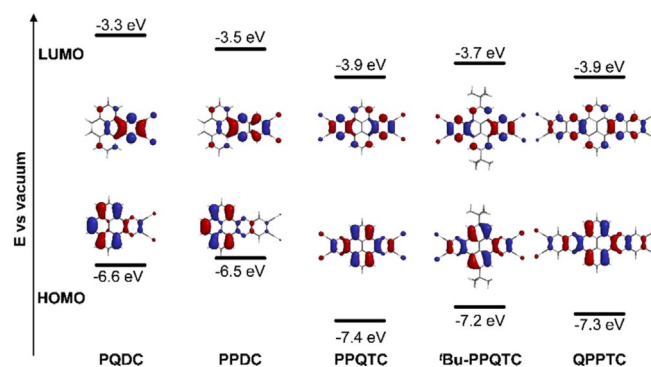

Figure 3. HOMO–LUMO diagrams of **PQDC**, **PPDC**, **H-PPQTC**, **tBu-PPQTC**, and **QPPTC** (calculated using DFT-B3LYP:6-311 + +G**).

Table 1. Optoelectronic and electrochemical properties of **PQDC**, **PPDC**, **H-PPQTC**, **tBu-PPQTC** and **QPPTC**.

Compound	λ_{abs} [c] [nm]	λ_{onset} [nm]	λ_{em} [nm] (λ_{ex}) [nm]	E_{Stokes} [cm^{-1}]	Φ [%]	$E_{g(opt)}$ [d] [eV]	E^{red} [e] [V]	EA [eV][f]	E_{HOMO}^{DFT} [g] [eV]	E_{LUMO}^{DFT} [g] [eV]	E_g^{DFT} [g] [eV]
PQDC[a]	447	492	510sh, 533 (445)	3609	31	2.5	−1.42	−3.4	−6.6	−3.3	3.3
PPDC[a]	485	514	534 (475)	1891	22	2.4	−1.32, −1.99	−3.5	−6.5	−3.5	3.0
H-PPQTC[a]	411	426	437 (401)	1448	37	2.9	−1.26, −1.49	−3.5	−7.4	−3.9	3.5
tBu-PPQTC[a]	418	437	461, 529 (408)	2231	15	2.8	−1.31, −1.54	−3.5	−7.2	−3.7	3.5
QPPTC[b]	440,[h] 412	451,[h]427	449,[h] 475, 526sh[i] (430)	455,[h] 3219	8.9	2.7,[h] 2.9	−1.74	−3.1	−7.3	−3.9	3.4

[a] Measured in CH_2Cl_2 at RT. [b] Measured in oDCB at RT. [c] absorption maximum at the longest wavelength. [d] Estimated from onset; $E_{g(opt)} = \frac{1242}{\lambda_{onset}}$. [e] Cyclic voltammogram measured with a Pt electrode and nBu_4NPF_6 as electrolyte. Scan speed: 50 mV s^{-1}; ferrocene/ferrocenium (Fc/Fc$^+$) was used as internal reference. [f] Electron affinity estimated by $EA = -(E_{red,1} + 4.8)$ eV. [g] Obtained from quantum-chemical calculations at the DFT-B3LYP/6-311 $+ +$ G** level of theory. [h] J-aggregate. [i] sh: shoulder.

Single-crystal X-ray structure analysis

Crystal packing plays a crucial role for charge-transport in organic semiconductors. For all compounds except **QPPTC**, single crystals were obtained by vacuum sublimation with a kugelrohrofen. Crystals were also grown from solution for **PQDC**, **H-PPQTC**, **tBu-PPQTC**, and **QPPTC**. In total, eight different modifications were obtained.

Crystals of **PQDC** were grown from solution, either by vapor diffusion of methanol into a THF solution or by slow evaporation of a CH_2Cl_2 solution, as well as by vacuum sublimation in a kugelrohrofen (200 °C, 5×10^{-3} mbar). In each case the same unit cell was obtained independent of the crystallization method, indicating that this packing motif is highly robust.

PQDC crystallized in the monoclinic space group $P2_1/c$ with four molecules per unit cell and one molecule in the asymmetric unit (polymorph α). Recently, the same packing and unit cell have been reported by Sutherland et al.[15] The cyano groups are slightly contorted out of planarity by approximately 2.5°. Adjacent molecules form π-stacked dimers, in which these are rotated by 120° (Figure 4 a). The molecules assemble in parallel one-dimensional π-stacked columns with $d_A = 3.38$ Å along the crystallographic c axis (Figure 4 b). Adjacent columns interact either by twofold hydrogen bonding between the cyano groups and aromatic protons ($d_B = 2.54$–2.58 Å), or to protons of the K-region ($d_C = 2.60$ Å, Figure 4 c). Similar twofold hydrogen-bonding motifs are known for other aromatic 1,2-dicyano compounds as well.[21]

However, when **PQDC** was crystallized by slow evaporation of a chloroform solution two different crystals were found in the same batch. One was identical with the previously described α modification. The other one was a different polymorph in monoclinic space group $P2_1/n$, with four molecules in the unit cell and one molecule in the asymmetric unit (polymorph β). Here, the molecules form two different face-to-face π-stacked dimers with antiparallel orientation of the two **PQDC** molecules and pronounced molecular overlap (Figure 4 d and e). Whereas dimer A_π has the longest π–π distance ($d_A = 3.51$ Å) of all structures in this work, dimer B_π has the shortest ($d_B = 3.29$ Å). **PQDC** forms one-dimensional stacks of alternating dimers A_π and B_π along the crystallographic a axis (Figure 4 f). These stacks are arranged in layers within the ab plane and interact through van der Waals interactions ($d_{ArH\cdots HAr} = 2.43$ Å). Adjacent layers are stabilized by triple hydrogen bonding of the cyano groups with aromatic protons ($d_{CN\cdots H} = 2.68$–2.81 Å, Figure 4 g). By using the UNI force field method[22] implemented in Mercury, intermolecular potentials between π-stacked dimers for both polymorphs were calculat-
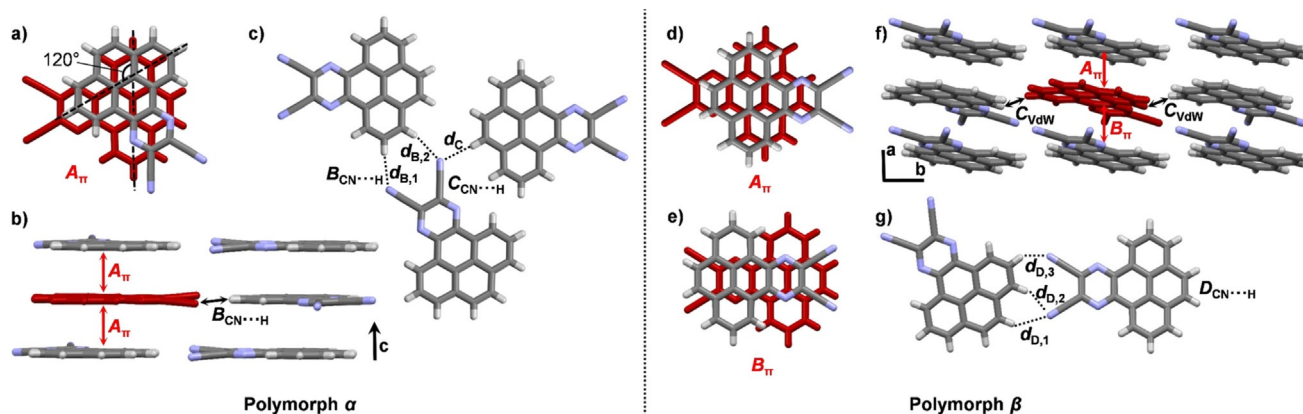

Figure 4. a–c) Single-crystal X-ray structure of **PQDC** (polymorph α) crystallized by sublimation in a kugelrohrofen (200 °C, 5×10^{-3} mbar), vapor diffusion of MeOH into a THF solution, or by evaporation of a CH_2Cl_2 solution. a) π-Stacked dimer A_π with $d_A = 3.38$ Å. b) Infinite face-to-face stacking pattern along the crystallographic c axis, indicated with red arrows. c) Hydrogen-bonding motif in dimers B and C ($d_{B,1} = 2.58$ Å, $d_{B,2} = 2.54$ Å, $d_C = 2.60$ Å. d)–g) Polymorph β crystallized by slow evaporation of a CHCl$_3$ solution. d),e) π-Stacked dimers A_π ($d_A = 3.51$ Å) and B_π ($d_B = 3.29$ Å). f) Infinite face-to-face stacking pattern along the crystallographic a axis, indicated with red arrows. g) Hydrogen-bonding motif in dimer D ($d_{D,1} = 2.81$ Å, $d_{D,2} = 2.68$ Å, $d_{D,1} = 2.79$ Å).

ed. In the α polymorph a potential of $E_\pi = -96\,\mathrm{kJ\,mol^{-1}}$ for dimer A was found; in the β polymorph the potentials are $E_\pi = -92\,\mathrm{kJ\,mol^{-1}}$ for dimer A_π and $E_\pi = -112\,\mathrm{kJ\,mol^{-1}}$ for dimer B_π. The total packing energies are similar for both modifications, that is, $E_{\mathrm{tot}} = -182\,\mathrm{kJ\,mol^{-1}}$ for α and $E_{\mathrm{tot}} = -187\,\mathrm{kJ\,mol^{-1}}$ for β, which explains the simultaneous competitive formation of both polymorphs from $\mathrm{CHCl_3}$. The robustness of the α polymorph under the other conditions seems to have kinetic rather than thermodynamic reasons.

Crystals of **PPDC** were grown by vacuum sublimation in a kugelrohrofen (250 °C, $(3$–$6)\times10^{-3}$ mbar). Like **PQDC**, **PPDC** also crystallized in monoclinic space group $P2_1/c$ with four molecules in the unit cell and one molecule in the asymmetric unit. The molecules assemble in π-stacked columns of two alternating dimers with $d_A = 3.34\,\text{Å}$ and $d_B = 3.37\,\text{Å}$ along the crystallographic b axis (Figure 5a–c). In both dimers the molecules are oriented in an antiparallel fashion and have a pronounced molecular overlap of the aromatic backbone (Figure 5a and b). Adjacent columns form a layered structure,
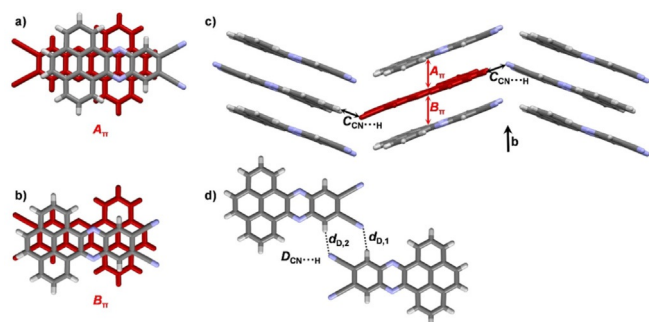
which is stabilized by hydrogen bonding between cyano groups and protons of the K-region. ($d_C = 2.47\,\text{Å}$, Figure 5c). Adjacent layers also form twofold hydrogen bonds ($d_D = 2.50\,\text{Å}$, Figure 5d). The parent structure of **PPDC** without cyano groups has been recently described:[15] π-stacked columns with a parallel orientation of the molecules. Thus, the antiparallel orientation observed in **PPDC** is related to the presence of the cyano groups and can be explained by the dipole moment induced by them favoring an alignment with close contacts of opposite poles.

For **H-PPQTC** two modifications could be obtained. The first one was grown by slow evaporation of a $\mathrm{CH_2Cl_2}$ solution (solvate α). Here **H-PPQTC** crystallized in triclinic space group $P\bar{1}$ with four molecules in the unit cell and two molecules in the asymmetric unit. Two solvent molecules are enclathrated as well. Two different π-stacked dimers can be found (Figure 6a and b). In dimer A_π adjacent molecules are twisted by approximately 90°, and in dimer B_π the twist angle is 63°. The π–π distance is the same for both dimers ($d_A = d_B = 3.38\,\text{Å}$). Both dimers form independent π-stacked columns along the crystallographic a axis (Figure 6c), which interact through dipolar CN···CN interactions ($d_{D1,2} = 3.49$–$3.55\,\text{Å}$) and hydrogen bonding ($d_{D,3} = 2.75\,\text{Å}$) between adjacent cyano groups and aromatic protons (Figure 6d).

Another polymorph of **H-PPQTC** was obtained by vacuum sublimation in a kugelrohrofen (300 °C, 5×10^{-2} mbar) (polymorph β). This time it crystallized in the orthorhombic space group $Pbca$ with eight molecules in the unit cell and one molecule in the asymmetric unit. Again, dimers with $d_A = 3.36\,\text{Å}$ and a twist of 62° (Figure 6e) very similar to dimer B_π found in the α modification are formed, which arrange in one-dimensional π-stacked columns along the crystallographic b axis (Figure 6f). The columns are aligned in layers in the crystallographic bc plane and are stabilized by dipolar C···N interactions ($d_B = 3.35$–$3.69\,\text{Å}$) between adjacent cyano groups (Figure 6g) and by twofold hydrogen bonding ($d_C = 2.65$–$2.69\,\text{Å}$, Figure 6h). Short

Figure 5. Single-crystal X-ray structure of **PPDC** (polymorph α) crystallized by sublimation in a kugelrohrofen (250 °C, $(3$–$6)\times10^{-3}$ mbar). a), b) π-Stacked dimers A_π ($d_A = 3.34\,\text{Å}$) and B_π ($d_B = 3.37\,\text{Å}$). c) Packing; asymmetric unit colored in red. Infinite face-to-face stacking pattern along the crystallographic b axis, indicated with red arrows. d) Twofold hydrogen-bonding motif in dimer D ($d_{D,1} = d_{D,2} = 2.50\,\text{Å}$).

Figure 6. a–d) Single-crystal X-ray structure of **H-PPQTC** (solvate α) crystallized by evaporation of a $\mathrm{CH_2Cl_2}$ solution. a), b) π-Stacked dimers A_π ($d_A = 3.38\,\text{Å}$) and B_π ($d_B = 3.38\,\text{Å}$). c) Packing; the colors correspond to molecules of the two different dimers shown in a) and b). Solvent molecules omitted for clarity. Infinite face-to-face stacking pattern along the crystallographic a axis, indicated with red and blue arrows. d) CN···CN short contacts and hydrogen-bonding motif in dimer D ($d_{D,1} = 3.49\,\text{Å}$, $d_{D,2} = 3.55\,\text{Å}$, $d_{D,3} = 2.75\,\text{Å}$). e–h) Polymorph β crystallized by sublimation in a kugelrohrofen (300 °C, 5×10^{-2} mbar). e) π-Stacked dimer A_π ($d_A = 3.36\,\text{Å}$). f) Packing; asymmetric unit colored in red. Infinite face-to-face stacking pattern along the crystallographic b axis, indicated with red arrows. g) CN···CN dipolar interaction motif B ($d_{B,1} = 3.58\,\text{Å}$, $d_{B,2} = 3.68\,\text{Å}$). h) Twofold hydrogen-bonding motif in dimer C ($d_{C,1} = 2.65\,\text{Å}$, $d_{C,2} = 2.69\,\text{Å}$).

Chemistry–A European Journal

Full Paper
doi.org/10.1002/chem.202002382

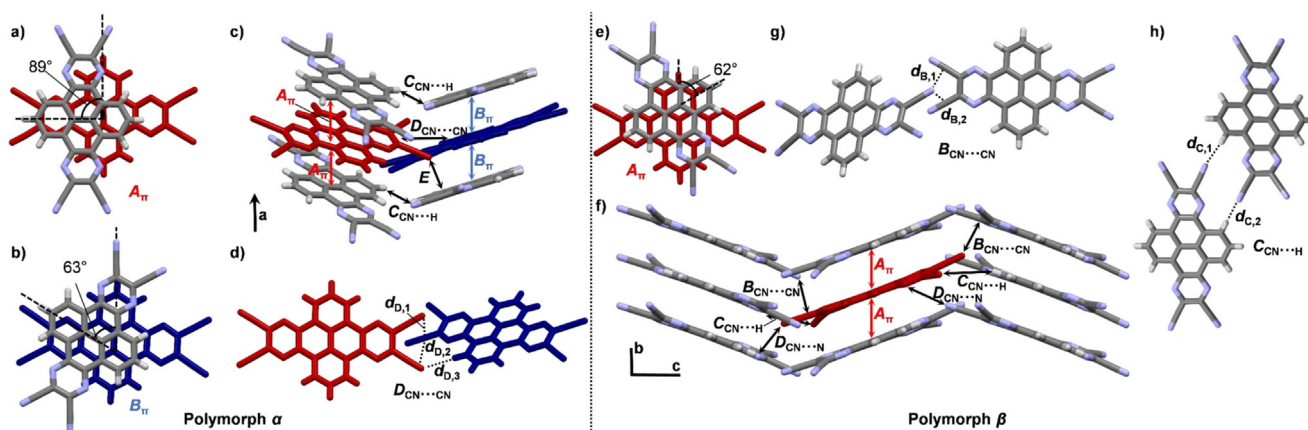**Chemistry Europe**
European Chemical
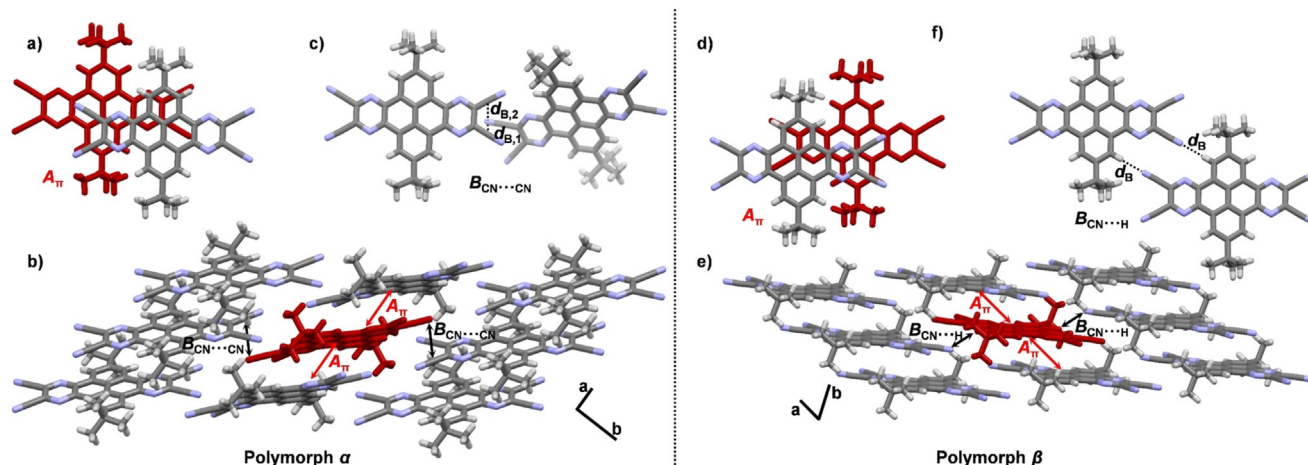Societies Publishing

Figure 7. a–c) Single-crystal X-ray structure of *t*Bu-PPQTC (solvate α) crystallized by evaporation of a CH_2Cl_2 solution. a) π-Stacked dimer A_π ($d_A = 3.36$ Å). b) Infinite face-to-face stacking pattern along the crystallographic *a* axis, indicated with red arrows. Solvent molecules omitted for clarity. c) CN···CN short-contact motif in dimer B ($d_{B,1} = 3.26$ Å, $d_{B,2} = 3.38$ Å). d–f) Polymorph β crystallized by sublimation in a kugelrohrofen (250 °C, 5×10^{-3} mbar). d) π-Stacked dimer A_π ($d_A = 3.37$ Å). e) Infinite face-to-face stacking pattern along the crystallographic *a* axis, indicated with red arrows. f) Twofold hydrogen-bonding motif in dimer B ($d_B = 2.73$ Å).

contacts between cyano groups and phenazine nitrogen atoms ($d_D = 3.48$ Å) are also found. Similar intermolecular potentials calculated by the UNI force field method exist for the π-stacked dimers (-116 to -120 kJ mol^{-1}) in both modifications, whereas the total packing energy is much higher for the solvate of the α polymorph with CH_2Cl_2 ($E_{tot} = -976$ kJ mol^{-1}) than for the structure of the sublimed β polymorph ($E_{tot} = -238$ kJ mol^{-1}), probably due to additional stabilization by interaction with the solvent molecules.

On slow evaporation of a solution in CH_2Cl_2, *t*Bu-PPQTC crystallized in the monoclinic space group $P2_1/n$ with four molecules in the unit cell and one molecule and one solvent molecule in the asymmetric unit (solvate α). The molecules form π-stacked dimers (Figure 7a) with $d_A = 3.36$ Å, which are arranged in one-dimensional columns along the crystallographic *a* axis. Adjacent columns form sheets in the crystallographic *ab* plane (Figure 7b), which are stabilized by dipolar CN···CN contacts ($d_B = 3.26$–3.66 Å) similar to those found in the previous structure (Figure 7c). Adjacent sheets interact through van der Waals interactions of the *tert*-butyl groups.

When sublimed in vacuo in a kugelrohrofen (250 °C, 5×10^{-3} mbar) *t*Bu-PPQTC crystallized in triclinic space group $P\bar{1}$ with one molecule per unit cell and half a molecule in the asymmetric unit (polymorph β). Similar to the α modification, π-stacked dimers (Figure 7d) with $d_A = 3.37$ Å form one-dimensional columns along the crystallographic *a* axis, which are arranged in sheets in the *ab* plane (Figure 7e). Within the sheets molecules interact through twofold hydrogen bonding ($d_B = 2.73$ Å) (Figure 7f). Adjacent sheets are stabilized by van der Waals interactions. Similar to the previous two structures the intermolecular potentials between the π-stacked dimers A are similar in both modifications (-140 to -143 kJ mol^{-1}), whereas the total packing energy is higher for the solvate α ($E_{tot} = -314$ kJ mol^{-1}) than for the sublimed polymorph β ($E_{tot} = -277$ kJ mol^{-1}). A comparison between the crystal structures of **H-PPQTC** and *t*Bu-PPQTC reveals that the *tert*-butyl groups in-

fluence the π stacking. Whereas **H-PPQTC** π stacks with a twist of the π planes of either 60 or 90°, parallel π stacking with smaller overlap of the planes is found in the presence of *tert*-butyl groups.

QPPTC was crystallized by slowly cooling a hot, saturated solution in benzonitrile. It crystallized in monoclinic space group $P2_1$ with two molecules of **QPPTC** and two solvent molecules in the asymmetric unit. One-dimensional π-stacked columns along the crystallographic *c* axis with $d_A = 3.40$ Å are formed (Figure 8a), with pronounced molecular overlap (Figure 8b). Adjacent columns are stabilized by a fourfold complementary combination of hydrogen bonding of the cyano nitrogen atom to the phenylene proton ($d_B = 2.58$–2.67 Å) and dipolar C···N interactions ($d_C = 3.39$–3.46 Å) (Figure 8c). Enclathrated benzonitrile molecules are strongly contorted out of planarity (Figure 8d), and this indicates that this fourfold interaction motif has a highly directing and stabilizing effect on the overall packing. Table 2 summarizes all crystallographic details.

The parent structure of **QPPTC** without cyano groups obtained by sublimation has already been described.[23] Here, columnar π stacks with similar molecular overlap and π–π dis-
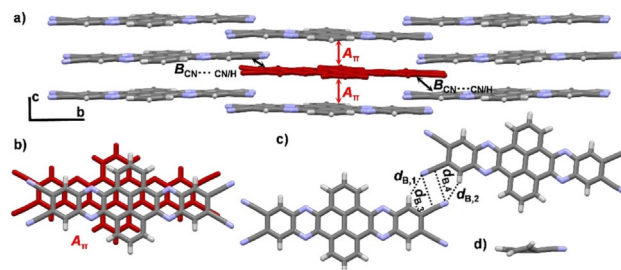
Figure 8. Single-crystal X-ray structure of **QPPTC** crystallized by cooling of a hot solution in benzonitrile. a) Infinite face-to-face stacking pattern along the crystallographic *c* axis, indicated with red arrows. Solvent molecules omitted for clarity. b) π-Stacked dimer A_π ($d_A = 3.40$ Å). c) Hydrogen-bonding and dipolar C···N interactions in dimer B ($d_{B,1} = 2.58$ Å, $d_{B,2} = 2.67$ Å, $d_{B,3} = 3.49$ Å, $d_{B,4} = 3.46$ Å). d) Contortion of enclathrated benzonitrile.

Table 2. Crystallographic parameters, distances, and short contacts of **PQDC**, **PPDC**, **H-PPQTC**, **tBu-PPQTC**, and **QPPTC**.[a]								
Compound	Method	Space group	N_{asym}[f]	Z[g]	$d_{\pi-\pi}$ [Å][h]	$\Theta_{\pi-\pi}$ [°][i]	$E_{\pi-\pi}$ [kJ mol^{-1}][j]	E_{tot} [kJ mol^{-1}][j]	Other short contacts [Å; °][a]
PQDC	THF/MeOH,[b] CH$_2$Cl$_2$, CHCl$_3$,[c] sublimation,[d] α	P2$_1$/c (monoclinic)	1	4	3.38	120	−96	−182	2.54–2.60; 115–135 (CN···H), 3.30; 146 (CN···N)
	CHCl$_3$,[c] β	P2$_1$/n (monoclinic)	1	4	3.51 (A), 3.29 (B)	180, 180	−92 (A), −112 (B)	−187	2.68–2.81; 107–160 (CN···H), 3.25; 105 (CN···N)
	sublimation[d]	P2$_1$/c (monoclinic)	1	4	3.34 (A), 3.37 (B)	180, 180	−116 (A), −118 (B)	−203	2.47–2.67; 110–136 (CN···H)
PPDC	CH$_2$Cl$_2$,[c] α	$P\bar{1}$ (triclinic)	4×0.5, 2×CH$_2$Cl$_2$	4	3.38 (A), 3.38 (B)	89, 63	−116 (A), −120 (B)	−976	3.42–3.82; 73–89 (CN···CN), 2.59–2.75; 128–132 (CN···H)
	sublimation,[d] β	Pbca (orthorhombic)	1	8	3.36	62	−118	−238	3.35–4.02; 81–113 (CN···CN), 2.49–2.69; 129–144 (CN···H), 3.12; 146 (CN···N)
H-PPQTC	CH$_2$Cl$_2$,[c] α	P2$_1$/n (monoclinic)	2×0.5, 1×CH$_2$Cl$_2$	4	3.37	0	−140	−314	3.26–3.66; 72–85 (CN···CN), 2.67; 152 (CN···H)
tBu-PPQTC	sublimation,[d] β	$P\bar{1}$ (triclinic)	0.5	1	3.37	0	−143	−277	2.73; 135.9 (CN···H)
QPPTC	benzonitrile[e]	P2$_1$ (monoclinic)	2, 2×C$_6$H$_5$CN	4	3.40	0	−178	−368	3.39–3.49, 88–94; 2.47–2.81; 127–142 (CN···H)

[a] Values were determined for two adjacent molecules. For the determination procedure, see the Supporting Information. [b] Vapor diffusion. [c] Slow evaporation at RT. [d] Under vacuum in a kugelrohrofen. [e] Cooling a hot, saturated solution to RT. [f] Number of molecules in the asymmetric unit; refined molecules of solvation not counted. [g] Total number of molecules in the unit cell including refined molecules of solvation. [h] The π–π distances; the numbers in parentheses indicate the π-stacking motifs shown in Figures 4–8; π distances were calculated as the mean distance of all atoms of the aromatic backbone (see the Supporting Information for details). [i] Torsion angle between two π-stacked molecules as shown in Figures 4–8. [j] Intermolecular potentials between π-stacked dimers and total packing energy calculated by the UNI force field method implemented in Mercury.[22]

tance (3.42 Å) are found that only differ in the relative orientation of the columns.

Calculated charge-transfer integrals

To evaluate the potential of the obtained structures for application as OFET materials, the electronic couplings between adjacent molecules of all obtained crystal structures were calculated. The electronic coupling (charge-transfer integral) between molecules can be used to quantify the charge-transport capability and depends on the relative orientation between the molecules. Different transfer integrals result in varying mobilities. For example, the charge-transport mobility in an anthracene crystal differs in different directions with respect to the orientation of the molecules.[24] Both HOMO transfer integrals t_h responsible for hole transport and LUMO transfer integrals t_e responsible for electron transport were calculated by the DFTB method (see the Supporting Information for details of the calculation).[25] The results for π-stacked dimers are listed in Table 3. Couplings of other molecular pairs with short contacts are negligibly small and are therefore not discussed herein (for details, see the Supporting Information). This also means that charge-carrier transport is expected to be highly anisotropic and occurs predominantly along the π-stacking axis, which is parallel to the shortest crystallographic axis in all structures, as indicated in Table 3. For most dimers in this work electron transport is favored over hole transport, as expected due to the electron-deficient nature of the compounds and the low-lying LUMOs.

For the α polymorph of **PQDC** a moderate coupling for electron transport ($t_e = 49$ meV) and a lower coupling for hole transport ($t_h = 20$ meV) were calculated for π-stacked molecules along the crystallographic c axis. For the β polymorph both electron and hole couplings are larger. Hole-transfer integrals for the two alternating π-stacked dimers along the a axis are $t_{h,A} = 88$ meV and $t_{h,B} = 57$ meV. For electron transport the transfer integrals are exceptionally large ($t_{e,A} = 113$ meV and $t_{e,B} = 252$ meV), which makes this polymorph highly promising for potential application in n-type OFETs. However, due to similar packing energies of both α and β polymorphs, polymorphic mixtures are to be expected, which is a drawback for device

Table 3. Charge transfer integrals for hole (t_h) and electron (t_e) transport for all crystal structures of **PQDC**, **PPDC**, **H-PPQTC**, **tBu-PPQTC**, and **QPPTC** and reorganization energies.						
Compound	Modification[a]	t_h[b] [meV]	t_e[b] [meV]	Direction[c]	λ_h[d] [meV]	λ_e[d] [meV]
PQDC	α	20	49	c		
	β	88 (A), 57 (B)	113 (A), 252 (B)	a	160	256
PPDC	α	13 (A) (B), 0	172 (A), 101 (B)	b	152	190
H-PPQTC	α	37 (A), 26 (B)	27 (A) (B), 46	a	136	121
	β	12	36	b		
tBu-PPQTC	α	53	76	a	141	129
	β	50	69	a		
QPPTC	α	4	108	c	117	91

[a] See Figures 4–8 and Table 2. [b] Transfer integral for hole (h) and electron (e) transport calculated by DFTB along the π-stacking axis. [c] Crystallographic axis parallel to π-stacking axis. [d] Reorganization energy for hole (h) and electron (e) transport calculated by DFT (B3LYP/6-31G*).

Chemistry–A European Journal

Full Paper
doi.org/10.1002/chem.202002382

Chemistry Europe
European Chemical
Societies Publishing

fabrication. For **PPDC**, too, an exceptionally large transfer integral for electron transport for dimer A_π (see Figure 5a) was found ($t_e = 172$ meV). For dimer B_π it is reduced to $t_e = 101$ meV, which is still a large value. Couplings in the same range have been previously reported for dimers of triptycene end-capped quinoxalino-phenanthrophenazines.[9aa] Both integrals are in the same range as for some perylene diimide derivatives (t_e up to 141 meV).[26] They are also similar to the transfer integral for hole transport of rubrene ($t_h = 100$ meV),[27] which is known to have excellent charge-carrier mobility in OFETs.[28] Since both dimers alternate along the crystallographic b axis, the coupling in dimer B_π most likely determines the overall charge transport. The large values make **PPDC** a promising candidate for potential application as an n-type semiconductor in OFET devices.[1] In contrast to the large transfer integrals for electron transport, couplings for hole transport are negligibly small (0–13 meV). For the α modification of **H-PPQTC** moderate couplings for both hole and electron transport were calculated along the a axis. They vary between $t_h = 37$ meV and $t_e = 27$ meV for dimer A_π and $t_h = 26$ meV and $t_e = 46$ meV for dimer B_π (see Figure 6a and b). Modification β has a similar integral for electron transport ($t_e = 36$ meV) and somewhat smaller integral for hole transport ($t_h = 12$ meV).

Both modifications of **tBu-PPQTC** show similar transfer integrals along the a axis. For hole transport they are $t_h = 50$ and 53 meV, whereas for electron transport fairly large couplings of $t_e = 69$ and 76 meV were obtained. These values are larger than those of **H-PPQTC** due to more efficient orbital interaction, and make **tBu-PPQTC** promising for potential device applications, whereas **H-PPQTC** seems to be unsuitable for efficient charge transfer. Thus, the addition of *tert*-butyl groups seems to be beneficial for this purpose. The longest fused aromatic system, namely **QPPTC**, shows a large electron-transfer integral along the crystallographic c axis (108 meV), whereas the hole coupling is negligible. This is contrary to the parent structure of **QPPTC** without cyano groups, for which hole-transfer integrals (63 meV) are much larger than those for electron transfer (14 meV).[23]

Reorganization energies for hole and electron transport were calculated as well (DFT/B3LYP-6-31G*). They describe the strength of local electron–phonon coupling and strongly affect the charge-transport properties.[29] Small energies are desired for high carrier mobilities.[14a, 30] The calculations revealed reorganization energies for hole transport between 117 and 160 meV, comparable to those of rubrene (159 meV)[31] and unsubstituted **QPP** (118 meV)[23] and slightly larger than that of pentacene (97 meV).[32]

For electron transport larger values were calculated for **PQDC** and **PPDC** (256 and 190 meV), whereas for the two **PPQTC** derivatives the energies were slightly smaller than for hole transport (121 and 129 meV). These values are rather low compared with electron-transfer reorganization energies of other systems, such as perylene diimides (250–322 mV)[26] **QPPTC** has the lowest reorganization energy (91 meV), which is only slightly higher than for its parent structure (80 meV).[23] Since for **QPPTC** reorganization energy is lower than the transfer integral, this should lead to very efficient bandlike charge transport, which is promising for high charge transport mobilities.[29b] Table 3 summarizes transfer integrals and reorganization energies.

Conclusions

The synthesis and optoelectronic characterization of five di- and tetracyanopyrazines was presented. Due to the electron-withdrawing effect of the cyano groups, all compounds have low-lying LUMO levels of up to −3.9 eV, making them predestined for electron transport. All compounds could be crystallized by vacuum sublimation and/or from solution. Single-crystal X-ray diffraction revealed in all eight structures columnar face-to-face π-stacking motifs with short π–π distances (≈ 3.29–3.51 Å; av 3.37 Å). Hydrogen-bonding and dipolar CN···CN interactions are found in all structures and seem to have a strong impact on stabilizing the packing. **PQDC** crystallized in the same unit cell regardless of the crystallization conditions. Only in the case of chloroform a second polymorph was also formed. For two compounds (i.e., **PPQTC** and **tBu-PPQTC**) two different modifications were obtained, but the π-stacking motifs were similar in both cases. Calculated charge-transfer integrals for electron transport of 69–76 meV for **tBu-PPQTC**, 101–172 meV for **PPDC**, 108 meV for **QPPTC** and 113–252 meV for **PQDC** (β), together with low reorganization energies (91–256 meV) indicate that those four compounds are promising candidates for n-type semiconductors. Their low molecular weight allows easy sublimation, which is beneficial both for purification and device fabrication. We are currently working on using these compounds in n-type OFET devices.

Conflict of interest

The authors declare no conflict of interest.

Keywords: aggregation · crystal engineering · electron transfer · fused-ring systems · pyrazaacenes

[1] a) X. Zhan, A. Facchetti, S. Barlow, T. J. Marks, M. A. Ratner, M. R. Wasielewski, S. R. Marder, *Adv. Mater.* **2011**, *23*, 268–284; b) C. R. Newman, C. D. Frisbie, D. A. da Silva Filho, J.-L. Brédas, P. C. Ewbank, K. R. Mann, *Chem. Mater.* **2004**, *16*, 4436–4451; c) J. Zaumseil, H. Sirringhaus, *Chem. Rev.* **2007**, *107*, 1296–1323; d) Y. Wen, Y. Liu, *Adv. Mater.* **2010**, *22*, 1331–1345; e) X. Zhao, X. Zhan, *Chem. Soc. Rev.* **2011**, *40*, 3728–3743.

[2] a) R.-P. Xu, Y.-Q. Li, J.-X. Tang, *J. Mater. Chem. C* **2016**, *4*, 9116–9142; b) A. Salehi, X. Fu, D.-H. Shin, F. So, *Adv. Funct. Mater.* **2019**, *29*, 1808803.

[3] a) Y. Min, C. Dou, D. Liu, H. Dong, J. Liu, *J. Am. Chem. Soc.* **2019**, *141*, 17015–17021; b) S. More, R. Bhosale, A. Mateo-Alonso, *Chem. Eur. J.* **2014**, *20*, 10626–10631.

Chemistry–A European Journal

Full Paper
doi.org/10.1002/chem.202002382

Chemistry
Europe
European Chemical
Societies Publishing

[4] D. M. de Leeuw, M. M. J. Simenon, A. R. Brown, R. E. F. Einerhand, *Synth. Met.* **1997**, *87*, 53–59.

[5] a) T. He, M. Stolte, F. Würthner, *Adv. Mater.* **2013**, *25*, 6951–6955; b) J. Soeda, T. Uemura, Y. Mizuno, A. Nakao, Y. Nakazawa, A. Facchetti, J. Takeya, *Adv. Mater.* **2011**, *23*, 3681–3685.

[6] a) G. Xue, J. Wu, C. Fan, S. Liu, Z. Huang, Y. Liu, B. Shan, H. L. Xin, Q. Miao, H. Chen, H. Li, *Mater. Horiz.* **2016**, *3*, 119–123; b) X. Xu, Y. Yao, B. Shan, X. Gu, D. Liu, J. Liu, J. Xu, N. Zhao, W. Hu, Q. Miao, *Adv. Mater.* **2016**, *28*, 5276–5283.

[7] C. Zhang, Y. Zang, E. Gann, C. R. McNeill, X. Zhu, C.-a. Di, D. Zhu, *J. Am. Chem. Soc.* **2014**, *136*, 16176–16184.

[8] a) M. L. Tang, J. H. Oh, A. D. Reichardt, Z. Bao, *J. Am. Chem. Soc.* **2009**, *131*, 3733–3740; b) A. S. Molinari, H. Alves, Z. Chen, A. Facchetti, A. F. Morpurgo, *J. Am. Chem. Soc.* **2009**, *131*, 2462–2463; c) M. C. R. Delgado, K. R. Pigg, D. A. da Silva Filho, N. E. Gruhn, Y. Sakamoto, T. Suzuki, R. M. Osuna, J. Casado, V. Hernández, J. T. L. Navarrete, N. G. Martinelli, J. Cornil, R. S. Sánchez-Carrera, V. Coropceanu, J.-L. Brédas, *J. Am. Chem. Soc.* **2009**, *131*, 1502–1512; d) J. Yin, K. Chaitanya, X.-H. Ju, *J. Mater. Res.* **2016**, *31*, 337–347.

[9] a) A. Mateo-Alonso, *Chem. Soc. Rev.* **2014**, *43*, 6311–6324; b) J. Hu, D. Zhang, S. Jin, S. Z. D. Cheng, F. W. Harris, *Chem. Mater.* **2004**, *16*, 4912–4915; c) J. Guo, Y. Xu, S. Jin, L. Chen, T. Kaji, Y. Honsho, M. A. Addicoat, J. Kim, A. Saeki, H. Ihee, S. Seki, S. Irle, M. Hiramoto, J. Gao, D. Jiang, *Nature Commun.* **2013**, *4*, 2736; d) A. Mateo-Alonso, N. Kulisic, G. Valenti, M. Marcaccio, F. Paolucci, M. Prato, *Chem. Asian J.* **2010**, *5*, 482–485; e) N. Kulisic, S. More, A. Mateo-Alonso, *Chem. Commun.* **2011**, *47*, 514–516; f) S. More, R. Bhosale, S. Choudhary, A. Mateo-Alonso, *Org. Lett.* **2012**, *14*, 4170–4173; g) R. García, M. Melle-Franco, A. Mateo-Alonso, *Chem. Commun.* **2015**, *51*, 8037–8040; h) A. B. Marco, D. Cortizo-Lacalle, C. Gozalvez, M. Olano, A. Atxabal, X. Sun, M. Melle-Franco, L. E. Hueso, A. Mateo-Alonso, *Chem. Commun.* **2015**, *51*, 10754–10757; i) G. Antonicelli, C. Gozalvez, A. Atxabal, M. Melle-Franco, L. E. Hueso, A. Mateo-Alonso, *Org. Lett.* **2016**, *18*, 4694–4697; j) D. Cortizo-Lacalle, A. Pertegás, M. Melle-Franco, H. J. Bolink, A. Mateo-Alonso, *Org. Chem. Front.* **2017**, *4*, 876–881; k) A. Mateo-Alonso, *Eur. J. Org. Chem.* **2017**, 7006–7011; l) D. Cortizo-Lacalle, C. Gozalvez, M. Melle-Franco, A. Mateo-Alonso, *Nanoscale* **2018**, *10*, 11297–11301; m) D. Cortizo-Lacalle, J. P. Mora-Fuentes, K. Strutyński, A. Saeki, M. Melle-Franco, A. Mateo-Alonso, *Angew. Chem. Int. Ed.* **2018**, *57*, 703–708; *Angew. Chem.* **2018**, *130*, 711–716; n) C. Gozalvez, J. L. Zafra, A. Saeki, M. Melle-Franco, J. Casado, A. Mateo-Alonso, *Chem. Sci.* **2019**, *10*, 2743–2749; o) J. P. Mora-Fuentes, A. Riaño, D. Cortizo-Lacalle, A. Saeki, M. Melle-Franco, A. Mateo-Alonso, *Angew. Chem. Int. Ed.* **2019**, *58*, 552–556; *Angew. Chem.* **2019**, *131*, 562–566; p) J. P. Mora-Fuentes, I. Papadopoulos, D. Thiel, R. Álvarez-Boto, D. Cortizo-Lacalle, T. Clark, M. Melle-Franco, D. M. Guldi, A. Mateo-Alonso, *Angew. Chem. Int. Ed.* **2020**, *59*, 1113–1117; *Angew. Chem.* **2020**, *132*, 1129–1133; q) B. Gao, M. Wang, Y. Cheng, L. Wang, X. Jing, F. Wang, *J. Am. Chem. Soc.* **2008**, *130*, 8297–8306; r) P. K. Sahoo, C. Giri, T. S. Haldar, R. Puttreddy, K. Rissanen, P. Mal, *Eur. J. Org. Chem.* **2016**, 1283–1291; s) J. Li, S. Chen, Z. Wang, Q. Zhang, *Chem. Rec.* **2016**, *16*, 1518–1530; t) Z. Wang, P. Gu, G. Liu, H. Yao, Y. Wu, Y. Li, G. Rakesh, J. Zhu, H. Fu, Q. Zhang, *Chem. Commun.* **2017**, *53*, 7772–7775; u) P.-Y. Gu, Z. Wang, G. Liu, H. Yao, Z. Wang, Y. Li, J. Zhu, S. Li, Q. Zhang, *Chem. Mater.* **2017**, *29*, 4172–4175; v) Z. Zhang, Q. Zhang, *Mater. Chem. Front.* **2020**, https://doi.org/10.1039/C9QM00656G; w) B.-L. Hu, K. Zhang, C. An, D. Schollmeyer, W. Pisula, M. Baumgarten, *Angew. Chem. Int. Ed.* **2018**, *57*, 12375–12379; *Angew. Chem.* **2018**, *130*, 12555–12559; x) B.-L. Hu, C. An, M. Wagner, G. Ivanova, A. Ivanova, M. Baumgarten, *J. Am. Chem. Soc.* **2019**, *141*, 5130–5134; y) B. Kohl, F. Rominger, M. Mastalerz, *Org. Lett.* **2014**, *16*, 704–707; z) B. Kohl, F. Rominger, M. Mastalerz, *Angew. Chem. Int. Ed.* **2015**, *54*, 6051–6056; *Angew. Chem.* **2015**, *127*, 6149–6154; aa) L. Ueberricke, D. Holub, J. Kranz, F. Rominger, M. Elstner, M. Mastalerz, *Chem. Eur. J.* **2019**, *25*, 11121–11134; ab) L. Ueberricke, S. Wieland, F. Rominger, M. Mastalerz, *Org. Mater.* **2019**, *01*, 050–062; ac) B. Kohl, F. Rominger, M. Mastalerz, *Chem. Eur. J.* **2015**, *21*, 17308–17313; ad) B. Kohl, M. V. Bohnwagner, F. Rominger, H. Wadepohl, A. Dreuw, M. Mastalerz, *Chem. Eur. J.* **2016**, *22*, 646–655; ae) B. Kohl, K.

[10] H. W. Rothkopf, D. Wöhrle, R. Müller, G. Koßmehl, *Chem. Ber.* **1975**, *108*, 875–886.

[11] E. Nardi, L. Chen, S. Clair, M. Koudia, L. Giovanelli, X. Feng, K. Müllen, M. Abel, *J. Phys. Chem. C* **2014**, *118*, 27549–27553.

[12] Q. Li, J. Li, H. Ren, Z. Gao, D. Liu, *Synth. Commun.* **2011**, *41*, 3325–3333.

[13] H. H. Abdel-Razik, K. H. Mahmoud, *J. Appl. Polym. Sci.* **2012**, *123*, 1329–1339.

[14] a) V. Coropceanu, J. Cornil, D. A. da Silva Filho, Y. Olivier, R. Silbey, J.-L. Brédas, *Chem. Rev.* **2007**, *107*, 926–952; b) C. Reese, Z. Bao, *J. Mater. Chem.* **2006**, *16*, 329–333.

[15] D. T. Hogan, B. S. Gelfand, D. M. Spasyuk, T. C. Sutherland, *Mater. Chem. Front.* **2020**, *4*, 268–276.

[16] J. Hu, D. Zhang, F. W. Harris, *J. Org. Chem.* **2005**, *70*, 707–708.

[17] T. Yamato, A. Miyazawa, M. Tashiro, *Chem. Ber.* **1993**, *126*, 2505–2511.

[18] R. Rieger, K. Müllen, *J. Phys. Org. Chem.* **2010**, *23*, 315–325.

[19] M. Halder, S. Datta, P. Bolel, N. Mahapatra, S. Panja, H. Vardhan, S. Kayal, D. K. Khatua, I. Das, *Anal. Methods* **2016**, *8*, 2805–2811.

[20] F. Würthner, T. E. Kaiser, C. R. Saha-Möller, *Angew. Chem. Int. Ed.* **2011**, *50*, 3376–3410; *Angew. Chem.* **2011**, *123*, 3436–3473.

[21] a) J. Janczak, R. Kubiak, *Acta Crystallogr. Sect. C* **1995**, *51*, 1399–1401; b) H. Li, F. R. Fronczek, M. G. H. Vicente, *J. Organomet. Chem.* **2009**, *694*, 1607–1611; c) Y. Zorlu, İ. Ün, C. Hirel, F. Dumoulin, V. Ahsen, *J. Chem. Crystallogr.* **2013**, *43*, 636–645.

[22] a) A. Gavezzotti, *Acc. Chem. Res.* **1994**, *27*, 309–314; b) A. Gavezzotti, G. Filippini, *J. Phys. Chem.* **1994**, *98*, 4831–4837.

[23] B. Wex, A. A. O. El-Ballouli, A. Vanvooren, U. Zschieschang, H. Klauk, J. A. Krause, J. Cornil, B. R. Kaafarani, *J. Mol. Struct.* **2015**, *1093*, 144–149.

[24] a) Y. Maruyama, H. Inokuchi, *Bull. Chem. Soc. Jpn.* **1967**, *40*, 2073–2077; b) R. G. Kepler, *Phys. Rev.* **1960**, *119*, 1226–1229.

[25] a) M. Elstner, D. Porezag, G. Jungnickel, J. Elsner, M. Haugk, T. Frauenheim, S. Suhai, G. Seifert, *Phys. Rev. B* **1998**, *58*, 7260–7268; b) A. Kubas, F. Hoffmann, A. Heck, H. Oberhofer, M. Elstner, J. Blumberger, *J. Chem. Phys.* **2014**, *140*, 104105; c) A. Kubas, F. Gajdos, A. Heck, H. Oberhofer, M. Elstner, J. Blumberger, *Phys. Chem. Chem. Phys.* **2015**, *17*, 14342–14354; d) A. Heck, J. J. Kranz, T. Kubař, M. Elstner, *J. Chem. Theory Comput.* **2015**, *11*, 5068–5082; e) A. Heck, J. J. Kranz, M. Elstner, *J. Chem. Theory Comput.* **2016**, *12*, 3087–3096; f) T. Kubař, M. Elstner, *J. Royal Soc. Interface* **2013**, *10*, 20130415; g) T. Kubař, M. Elstner, *J. Phys. Chem. B* **2010**, *114*, 11221–11240; h) G. Lüdemann, I. A. Solov'yov, T. Kubař, M. Elstner, *J. Am. Chem. Soc.* **2015**, *137*, 1147–1156; i) G. Lüdemann, P. B. Woiczikowski, T. Kubař, M. Elstner, T. B. Steinbrecher, *J. Phys. Chem. B* **2013**, *117*, 10769–10778; j) D. Holub, H. Ma, N. Krauß, T. Lamparter, M. Elstner, N. Gillet, *Chem. Sci.* **2018**, *9*, 1259–1272; k) B. Aradi, B. Hourahine, T. Frauenheim, *J. Phys. Chem. A* **2007**, *111*, 5678–5684.

[26] M. C. R. Delgado, E.-G. Kim, D. A. d. S. Filho, J.-L. Bredas, *J. Am. Chem. Soc.* **2010**, *132*, 3375–3387.

[27] K. A. McGarry, W. Xie, C. Sutton, C. Risko, Y. Wu, V. G. Young, J.-L. Brédas, C. D. Frisbie, C. J. Douglas, *Chem. Mater.* **2013**, *25*, 2254–2263.

[28] V. C. Sundar, J. Zaumseil, V. Podzorov, E. Menard, R. L. Willett, T. Someya, M. E. Gershenson, J. A. Rogers, *Science* **2004**, *303*, 1644–1646.

[29] a) K. Sakanoue, M. Motoda, M. Sugimoto, S. Sakaki, *J. Phys. Chem. A* **1999**, *103*, 5551–5556; b) E.-G. Kim, V. Coropceanu, N. E. Gruhn, R. S. Sánchez-Carrera, R. Snoeberger, A. J. Matzger, J.-L. Brédas, *J. Am. Chem. Soc.* **2007**, *129*, 13072–13081.

[30] J.-L. Brédas, D. Beljonne, V. Coropceanu, J. Cornil, *Chem. Rev.* **2004**, *104*, 4971–5004.

[31] D. A. da Silva Filho, E.-G. Kim, J.-L. Brédas, *Adv. Mater.* **2005**, *17*, 1072–1076.

[32] V. Coropceanu, O. Kwon, B. Wex, B. R. Kaafarani, N. E. Gruhn, J. C. Durivage, D. C. Neckers, J.-L. Brédas, *Chem. Eur. J.* **2006**, *12*, 2073–2080.